ISSN 0967-0912, Steel in Translation, 2015, Vol. 45, No. 1, pp. 54–62. © Allerton Press, Inc., 2015.
Original Russian Text © E.E. Merker, E.A. Chermenev, 2015, published in "Stal'," 2015, No. 1, pp. 23–31.

Energy-Efficient Melting of Reduced Iron-Ore Pellets in an Arc Furnace

E. E. Merker and E. A. Chermenev

Staryi Oskol Technological Institute, Moscow Institute of Steel and Alloys, Staryi Oskol, Russia
e-mail: fenix-evg@yandex.ru

Abstract—The melting of reduced iron-ore pellets in an arc furnace is considered. The refined model of the combined heating and melting of the pellets takes account of the action of the electrical arc close to the electrodes and the formation of a solid crust. Simulation indicates that the melting of pellets close to the electrodes intensifies the electrosmelting of steel, with clear economic benefits.

Keywords: arc furnace, pellet heating, pellet melting, electrical arc

DOI: 10.3103/S0967091215010106

The electrosmelting of pellets in an arc furnace with tubular (hollow) electrodes is promising [1–3]. For reduced iron-ore pellets, the electrosmelting characteristics will depend on the heat generation and heat transfer in the high-temperature furnace arc and on the heating and melting of the pellets within the slag–metal melt under the action of the arc [1].

When the pellets are supplied to the region affected by the arc through the tubular electrodes, their heating and melting will be more rapid, thanks to the additional heating on passing through the arc and the high-temperature melt in the zone around the arc, as follows from experimental data regarding the melting of reduced iron-ore pellets in a 150-t arc furnace [1, 2]. This process is more efficient than other electrosmelting technologies [1, 4].

As for steel scrap, the interaction of the pellets with the liquid metal is a complex heat- and mass-transfer process and is nonsteady, in general [4]. The heating and melting of the pellets within the slag–metal melt when they are introduced in the bath by different methods must be analyzed in more detail. A mathematical model for the heating and melting of pellets in the arc–slag–metal system may be derived on the basis of data regarding their electrosmelting in arc furnaces [5], the interaction of a solid with ferrocarbon melt [4], the formation of a coating on the pellet surface on entering the bath [6], and the intensification of pellet melting in slag–metal melt close to the arc [1, 5].

In the analysis of pellet melting, we must consider a heat-conduction problem with a moving boundary. Numerical methods of solving such significantly nonlinear problems are relatively well-developed. Versions of the finite-difference method are mainly employed [4, 7]. In formulating a mathematical model, we adopt a number of assumptions and constraints [1, 6, 8]. We must take into account that the phase transformations that accompany the cooling and heating processes associated with pellet melting give rise to a nonlinear heat-conduction problem [7].

Consider the internal heat transfer when pellets are supplied to the bath of the arc furnace through tubular electrodes [1]. In that case, the pellets initially undergo intense irradiation when they pass close to the electric arc; the melting point of the metal is higher than that of the pellets. The melting process includes the following stages.

(1) Surface heating of the falling pellet to the melting point as a result of irradiation by the arc.

(2) Melting of the pellet in the arc close to the electrode as it falls. The pellet melt accumulates at the surface of the solid residue, is heated above the melting point, and transfers heat from the surface irradiated by the arc.

(3) Melting of the pellet in the liquid metal close to the electrodes. (The formation of a metal crust is possible).

In this case, the temperature field in the first stage (heating) corresponds to a one-dimensional heat-conduction equation in spherical coordinates

$$c\rho\frac{\partial t}{\partial \tau} = \frac{1}{r^2}\frac{\partial}{\partial r}\left(r^2\lambda\frac{\partial t}{\partial r}\right) \text{ when } 0 < r < r_{pe}, \qquad (1)$$

where λ is the thermal conductivity, W/m °C; c is the specific heat, J/kg °C; ρ is the density of the elementary layer, kg/m^3; r_{pe} is the initial pellet radius, m.

The initial condition is the initial temperature distribution over the pellet cross section. Initially, the body is uniformly heated

$$t(r, 0) = t_0 \text{ when } 0 \le r \le r_{pe}, \qquad (2)$$

where t_0 is the initial pellet temperature, °C.

For all three stages, the boundary condition at the center (when $r = 0$) is a consequence of the temperature field's symmetry

$$\partial t(0, \tau)/\partial r = 0. \quad (3)$$

We may identify two boundary conditions at the surface (when $r = r_{pe}$). First, the surface is heated to the phase-transition temperature at the end of the stage

$$t(r_{pe}, \tau) = t_{me}, \quad (4)$$

where t_{me} is the pellet's melting point, °C. The second corresponds to the thermal balance at the pellet surface

$$\lambda \frac{\partial t(r_{pe}, \tau)}{\partial r} = q_{rad}, \quad (5)$$

where q_{rad} is the radiant heat flux from the arc to the pellet surface.

Since the melt formed in the second stage remains at the pellet surface and, by assumption, its density remains unchanged, the temperature field satisfies Eq. (1) but for the pellet in the region $0 < r < r_{sur}(\tau)$ and for the melt in the region $r_{sur}(t) < r < r_{pe}$. Here $r_{sur}(t)$ is the surface radius of the pellet's solid core, characterizing the motion of the solid–liquid boundary; it must be determined in solving the problem. We have two boundaries: the moving boundary between the pellet's solid core and the melt; and the constant boundary at the irradiated melt surface. The initial conditions here are the temperature distribution over the pellet cross section at the end of the first stage; and the pellet radius.

The first boundary condition is that the phase transitions at the moving boundary occur at specific temperatures, in accordance with Eq. (4). The second condition is the heat balance at the moving boundary

$$\lambda \frac{\partial t(r_{sur}(\tau), t)}{\partial r} - \rho L v_{me} = 0, \quad (6)$$

where v_{me} is the bulk rate of melting, m³/s; L is the melt's latent heat of phase transformation (melting), J/kg. The boundary condition at the melt surface (at $r = r_{pe}$) is analogous to Eq. (5).

In the third stage, in contrast to the second, the temperature field, which satisfies Eq. (1), is only considered within the solid residue: $0 < r < r_{sur}(\tau)$. There are two initial conditions: the temperature distribution over the pellet cross section; and the radius of the solid residue. The second boundary condition is the heat balance at the pellet–melt boundary

$$-\lambda \frac{\partial t(r_{sur}(\tau), t)}{\partial r} + q_0 \pm \rho L v_{me} = 0, \quad (7)$$

where $q_0 = \alpha(t_{melt} - t_{sur})$ is the heat flux from the melt to the pellet surface, W/m²; α is the convective heat-transfer coefficient, W/m² °C: t_{melt} is the melt temperature, °C; t_{sur} is the surface temperature, °C.

To solve the problem, we use a grid with a variable number of points. We assume that the boundary moves over one coordinate increment within a single time increment. In other words, the number of increments with respect to the coordinate n_k changes by one: on solidification, $n_{k+1} = n_k + 1$; on melting, $n_{k+1} = n_k - 1$.

In the derivation of the difference equation for the second stage, corresponding to Eq. (6), we assume that, in one time step, the boundary moves by one coordinate step. In this case, however, when the number of increments with respect to the coordinate decreases by one for the pellet, the number of corresponding increments for the melt increases by one. Thus, the total number of increments remains unchanged. In this approach, the time step is unknown and must be calculated. Therefore, we use unconditional stable implicit difference schemes in that case. To simulate pellet melting, we use an implicit four-point difference scheme, which is less complex than a six-point scheme [7]. In constructing the difference scheme, we use the balance method. The starting point is conservation of energy and the heat transfer corresponding to the discrete temperature field.

Consider an elementary layer $r_{i-1/2} < r < r_{i+1/2}$ (thickness Δr), corresponding to some point i (shaded in Fig. 1a). We write the corresponding heat-balance equation on transition from time k to time $k + 1$

$$(t_i^{k+1} - t_i^k)(c_i^+ \rho_i^+ V_i^+ + c_i^- \rho_i^- V_i^-) = (q_{i-1/2} F_{i-1/2} + q_{i+1/2} F_{i+1/2}) \Delta\tau, \; i = 2, \ldots, n_k, \quad (8)$$

where $q_{i-1/2}$, $q_{i+1/2}$ are the heat fluxes entering elementary layer i from the adjacent points on the left and right, respectively, W. In addition

$$F_{i-1/2} = 4\pi(r_i - \Delta r/2)^2,$$
$$F_{i+1/2} = 4\pi(r_i + \Delta r/2)^2$$

are the areas of the left and right surfaces of elementary layer i, respectively, m², while

$$V_i^- = (4/3)\pi[r_i^3 - (r_i - \Delta r/2)^3],$$
$$V_i^+ = (4/3)\pi[(r_i - \Delta r/2)^3 - r_i^3]$$

are the volumes of the left and right sections of elementary layer i, respectively, m³; c_i^-, ρ_i^-, λ_i^-, and c_i^+, ρ_i^+, λ_i^+ are thermophysical properties of the left (–) and right (+) sections of elementary layer i; r_i is the radius of elementary layer i, m; Δ_r is the coordinate (radius) increment, m; t_i^k is the temperature of elementary layer i at time k, °C; $\Delta\tau$ is the time increment, s.

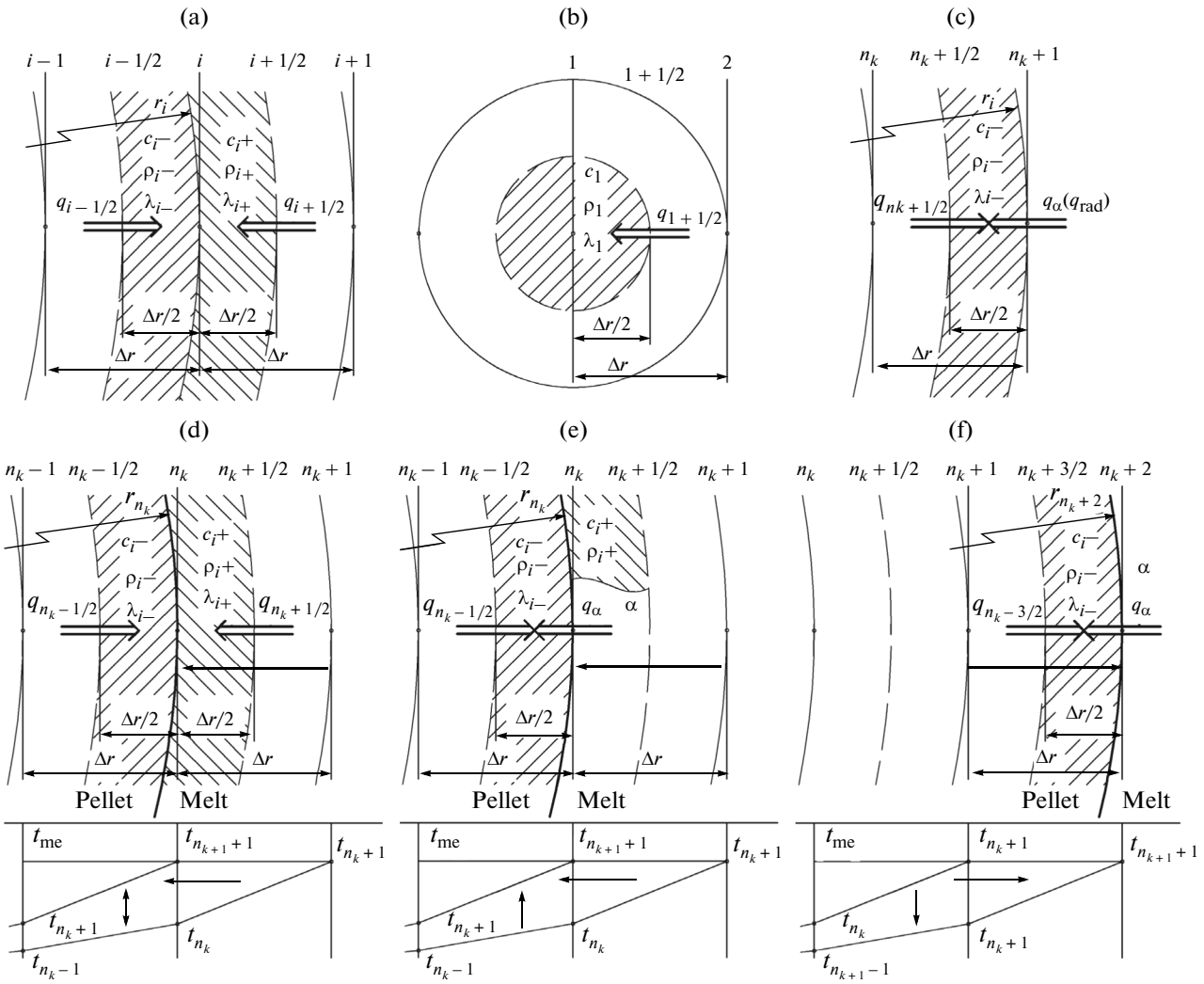

Fig. 1. Formulating the thermal balance: (a) elementary layer i of pellet; (b) center of pellet; (c) pellet surface; (d) at the moving phase boundary of a pellet melting in the arc; (e, f) external layer in melting and solidification, respectively.

The right side of Eq. (8) expresses the quantity of heat obtained by elementary layer (point) i in time interval $\Delta\tau$. The left side expresses the change in enthalpy of the elementary layer i with change in its temperature from t_i^k to t_i^{k+1}. To obtain a closed system of difference equations in terms of the grid temperature values, we relate the heat-flux density to the temperature at particular grid points. This calls for a discrete analog of the Fourier law. We use an implicit four-point difference scheme; therefore, we adopt the temperature at the subsequent time $k + 1$

$$\begin{aligned} q_{i-1/2} &= \lambda_i^-(t_{i-1}^{k+1} - t_i^{k+1})/\Delta r, \\ q_{i+1/2} &= \lambda_i^+(t_{i+1}^{k+1} - t_i^{k+1})/\Delta r. \end{aligned} \tag{9}$$

If we substitute Eq. (9) into Eq. (8), we obtain the discrete analog of Eq. (1)

$$\begin{aligned} &[(t_i^{k+1} - t_i^k)/\Delta\tau][4\pi c_i^+\rho_i^+((r_i + \Delta r/2)^3 - r_i^3)/3 \\ &\quad + 4\pi c_i^-\rho_i^-(r_i^3 - (r_i - \Delta r/2)^3)/3] \\ &= 4\pi\lambda_i^-(t_{i-1}^{k+1} - t_i^{k+1})(r_i - \Delta r/2)^2/\Delta r \\ &\quad + 4\pi\lambda_i^+(t_{i+1}^{k+1} - t_i^{k+1})(r_i + \Delta r/2)^2\Delta r, \\ &\quad i = 2, \ldots, n_k(\tau). \end{aligned} \tag{10}$$

The difference equations for the left boundary point ($i = 1$) corresponding to the boundary condition at the center of the pellet in Eq. (3) may be obtained by writing the heat balance for an elementary sphere of radius $\Delta r/2$ (Fig. 1b)

$$\begin{aligned} &[(t_i^{k+1} - t_i^k)/\Delta\tau]4\pi c_1\rho_1(\Delta r/2)^3/3 \\ &= 4\pi\lambda_1(t_2^{k+1} - t_1^{k+1}(\Delta r/2)^2/\Delta r). \end{aligned} \tag{11}$$

For the right boundary condition ($i = n_k + 1$), we write a difference equation corresponding to Eq. (4) at the pellet's phase boundary

$$t^{k+1}_{n_{k+1}+1} = t_{\text{me}}. \tag{12}$$

In the first stage, the difference equation for the right boundary point ($i = n + 1$) corresponding to Eq. (5) may be obtained if we write the thermal balance for an elementary surface layer of thickness $\Delta r/2$ (Fig. 1c)

$$\begin{aligned}&[(t^{k+1}_{n_k+1} - t^{k}_{n_k+1})/\Delta\tau]4\pi c^{-}_{n_k+1}\rho^{-}_{n_k+1}\\ &\times (r^3_{n_k+1} - (r_{n_k+1} - \Delta r/2)^3)/3\\ &= 4\pi\lambda^{-}_{n_k+1}(t^{k+1}_{n_k} - t^{k+1}_{n_k+1})(r_{n_k+1} - \Delta r/2)^2/\Delta r + q_{\text{rad}}.\end{aligned} \tag{13}$$

In the second stage, the heat flux from the melt is greater than the flux from the phase boundary to the center of the pellet. To obtain the difference analog of Eq. (6), we write the thermal balance for the new boundary point, corresponding to elementary layer $n_{k+1} + 1$ (Fig. 1d)

$$\begin{aligned}&4\pi\lambda^{-}_{n_k}(t^{k+1}_{n_{k+1}} - t^{k+1}_{n_{k+1}+1})(r_{n_k} - \Delta r/2)^2/\Delta r + 4\pi\lambda^{+}_{n_k}\\ &\times (t^{k+1}_{n_{k+1}+2} - t^{k+1}_{n_{k+1}+1})(r_{n_k} + \Delta r/2)^2/\Delta r\\ &+ \frac{4}{3}\pi\rho^{+}_{n_k}L^{+}_{n_k}\frac{(r_{n_{k+1}} - \Delta r)^3 - r^3_{n_{k+1}}}{\Delta\tau} - \frac{t^{k+1}_{n_k} - t^{k}_{n_k}}{\Delta\tau}\\ &\times \{4\pi c^{+}_{n_k}L^{+}_{n_k}[(r_{n_k} + \Delta r/2)^3 - r^3_{n_k}]/3\\ &+ 4\pi c^{-}_{n_k}\rho^{-}_{n_k}[r^3_{n_k} - (r_{n_k} - \Delta r/2)^3]/3\} = 0.\end{aligned} \tag{14}$$

The last term corresponds to the heat flux consumed in heating the elementary layer $n_{k+1} + 1$ (shaded area in Fig. 1d) to the melting point. The third term corresponds to melting of the elementary layer to the right of the new boundary point.

To obtain the difference analog of Eq. (7) for the third stage, we write the thermal balance for the new boundary point corresponding to elementary layer $n_{k+1} + 1$. In melting of the layer ($n_{k+1} = n_k - 1$), the external heat flux is greater than the heat flux from the phase boundary (Fig. 1e)

$$\begin{aligned}&4\pi\frac{\lambda^{-}_{n_k}}{\Delta r}(t^{k+1}_{n_{k+1}} - t^{k+1}_{n_{k+1}+1})(r_{n_k} - \Delta r/2)^2 + 4\pi\alpha(t_p - t^{k+1}_{n_k})\\ &\times r^2_{n_k} + \frac{4}{3}\pi\rho^{+}_{n_k}L^{+}_{n_k}\frac{(r_{n_{k+1}} - \Delta r)^3 - r^3_{n_{k+1}}}{\Delta\tau}\\ &- \frac{t^{k+1}_{n_k} - t^{k}_{n_k}}{\Delta\tau}\left\{\frac{4}{3}\pi c^{+}_{n_k}\rho^{+}_{n_k}[(r_{n_k} + \Delta r/2)^3 - r^3_{n_k}]\right.\\ &\left.+ \frac{4}{3}\pi c^{-}_{n_k}\rho^{-}_{n_k}[r^3_{n_k} - (r_{n_k} - \Delta r/2)^3]\right\} = 0.\end{aligned} \tag{15}$$

The last term corresponds to the heat flux consumed in heating the elementary layer $n_{k+1} + 1$ (shaded area in Fig. 1e) to the melting point. The third term corresponds to melting of the elementary layer to the right of the new boundary point.

In solidification of the elementary layer ($n_{k+1} = n_k + 1$), the external heat flux is less than the heat flux from the phase boundary (Fig. 1f)

$$\begin{aligned}&4\pi\lambda^{-}_{n_k+2}(t^{k+1}_{n_{k+1}} - t^{k+1}_{n_{k+1}+1})(r_{n_k+2} - \Delta r/2)^2/\Delta r\\ &+ 4\pi\alpha(t_p - t^{k+1}_{n_k+2})r^2_{n_k+2} + \frac{4}{3}\pi\rho^{-}_{n_k+2}L^{-}_{n_k+2}\\ &\times \frac{(r_{n_k+1} + \Delta r)^3 - r^3_{n_k+1}}{\Delta\tau} = 0.\end{aligned} \tag{16}$$

We may write Eqs. (10)–(16) in more compact form by introducing the thermal diffusivity $a = \lambda/c\rho$; the dimensionless temperature $\theta = (t - t_0)/(t_{\text{me}} - t_0)$; the coordinate $x = r/r_{\text{pe}}$; the Fourier time $\text{Fo} = a\tau/r^2_{\text{pe}}$; the Kirpichev number $\text{Ki} = r_{\text{pe}}q_0/\lambda(t_{\text{me}} - t_0)$; the Kosovich number $\text{Ko} = \rho' L/c\rho(t_{\text{me}} - t_0)$; and the dimensionless variables

$$K_\lambda = \lambda'/\lambda,\ K_{c\rho} = c'\rho'/(c\rho)$$

$$\text{and } K_{\text{rad}} = q_{\text{rad}}/[4\pi r_{\text{pe}}\lambda(t_{\text{me}} - t_0)].$$

We find that

$$\begin{aligned}&[(\theta^{k+1}_i - \theta^{k}_i)/(3\Delta\text{Fo})][K^{+}_{c\rho,i}(x_i + \Delta x/2)^3\\ &- K^{-}_{c\rho,i}(x_i - \Delta x/2)^3 + x^3_i(K^{-}_{c\rho,i} - K^{+}_{c\rho,i})]\\ &= K^{-}_{\lambda,i}(\theta^{k+1}_{i-1} - \theta^{k+1}_i)(x_i - \Delta x/2)^2/\Delta x\\ &+ K^{+}_{\lambda,i}(\theta^{k+1}_{i+1} - \theta^{k+1}_i)(x_i - \Delta x/2)^2/\Delta x;\end{aligned} \tag{17}$$

$$\begin{aligned}&[(\theta^{k+1}_1 - \theta^{k}_1)/(3\Delta\text{Fo})]K_{c\rho,1}(\Delta x/2)^3\\ &= K_{\lambda,1}(\theta^{k+1}_2 - \theta^{k}_1)(\Delta x/2)^3/\Delta x;\end{aligned} \tag{18}$$

$$\theta^{k+1}_{n_{k+1}+1} = \theta_{\text{me}}. \tag{19}$$

For the first stage

$$\begin{aligned}&[(\theta^{k+1}_{n_k+1} - \theta^{k}_{n_k+1})/(3\Delta\text{Fo})]K^{-}_{c\rho,n_k+1}\\ &\times [x^3_{n_k+1} - (x_{n_k+1} - \Delta x/2)^3] = K^{-}_{\lambda,n_k+1}(\theta^{k+1}_{n_k} - \theta^{k}_{n_k+1})\\ &\times (x_{n_k+1} - \Delta x/2)^2/\Delta x + K_{\text{rad}}.\end{aligned} \tag{20}$$

For the second stage

$$\begin{aligned}&K^{-}_{\lambda,n_k}(\theta^{k+1}_{n_{k+1}} - \theta^{k}_{n_{k+1}+1})(x_{n_k} - \Delta x/2)^2/\Delta x\\ &+ K^{+}_{\lambda,n_k}(\theta^{k+1}_{n_{k+1}+2} - \theta^{k}_{n_{k+1}+1})(x_{n_k} + \Delta x/2)^2/\Delta x\\ &+ \text{Ko}\frac{(x_{n_k+1} - \Delta x)^3 - x^3_{n_k+1}}{3\Delta\text{Fo}} - \frac{\theta^{k+1}_{n_k} - \theta^{k}_{n_k}}{3\Delta\text{Fo}}\\ &\times \left[K^{+}_{c\rho,n_k}\left(x_{n_k} + \frac{\Delta x}{2}\right)^3 - K^{-}_{c\rho,n_k}\left(x_{n_k} + \frac{\Delta x}{2}\right)^3\right.\\ &\left.+ x^3_{n_k}(K^{-}_{c\rho,n_k} - K^{+}_{c\rho,n_k})\right] = 0.\end{aligned} \tag{21}$$

For the third stage when the layer is melting

$$K^-_{\lambda,n_k}(\theta^{k+1}_{n_{k+1}}-\theta^{k}_{n_{k+1}+1})(x_{n_k}-\Delta x/2)^2/\Delta x+\mathrm{Kix}^2_{n_k}+\mathrm{Ko}\frac{(x_{n_{k+1}}-\Delta x)^3-x^3_{n_k+1}}{3\Delta\mathrm{Fo}}-\frac{\theta^{k+1}_{n_k}-\theta^{k}_{n_k}}{3\Delta\mathrm{Fo}}\times[K^+_{c\rho,n_k}(x_{n_k}+\Delta x/2)^3-K^-_{c\rho,n_k}(x_{n_k}-\Delta x/2)^3+x^3_{n_k}(K^-_{c\rho,n_k}-K^+_{c\rho,n_k})]=0. \quad (22)$$

For the third stage when the layer is solidifying

$$K^-_{\lambda,n_k+2}(\theta^{k+1}_{n_{k+1}}-\theta^{k}_{n_{k+1}+1})(x_{n_k+2}-\Delta x/2)^2/\Delta x+\mathrm{Kix}^2_{n_k+2}+\mathrm{Ko}\frac{(x_{n_k+1}+\Delta x)^3-x^3_{n_k+1}}{3\Delta\mathrm{Fo}}=0. \quad (23)$$

Let

$$K_{V_i}=[K^+_{c\rho,i}(x_i+x/2)^3-K^-_{c\rho,i}(x_i-x/2)^3+x^3(K^-_{c\rho,i}-K^+_{c\rho,i})]/3;$$

$$K_{V_{n_k+1}}=K^-_{c\rho,n_k}[x^3_{n_k+1}-(x_{n_k+1}-\Delta x/2)^3]/3;$$

$$Kl_i=K^-_{\lambda,i}(x_i-\Delta x/2)^2/\Delta x;$$

$$Kr_i=K^+_{\lambda,i}(x_i+\Delta x/2)^2/\Delta x;$$

$$K_{Vl}=[(X_{n_k+1}-\Delta x)^3-x^3_{n_k+1}]/3;$$

$$K_{Vh}=\left[K^+_{c\rho,n_k}\left(x_{n_k}+\frac{\Delta x}{2}\right)^3-K^-_{c\rho,n_k}\left(x_{n_k}-\frac{\Delta x}{2}\right)^3+x^3_{n_k}(K^-_{c\rho,n_k}-K^+_{c\rho,n_k})\right]\Big/3;$$

$$K_{Vs}=[(x_{n_k+1}+\Delta x)^3-x^3_{n_{k+1}}]/3.$$

We may now write Eqs. (17), (18), and (20)–(23) in the form

$$(\theta^{k+1}_i-\theta^k_i)K_{V_i}/\Delta\mathrm{Fo}=(\theta^{k+1}_{i-1}-\theta^k_i)Kl_i+(\theta^{k+1}_{i+1}-\theta^k_i)Kr_i, \quad (24)$$

$$(\theta^{k+1}_i-\theta^k_i)/\Delta\mathrm{Fo}=K_{\lambda,1}+(\theta^{k+1}_2-\theta^k_1)\times 6/(K_{c\rho,1}\Delta x^2). \quad (25)$$

For the first stage

$$(\theta^{k+1}_{n_k+1}-\theta^k_{n_k+1})K_{V_{n_k+1}}/\Delta\mathrm{Fo}=Kl_{n_k+1}(\theta^{k+1}_{n_k}-\theta^k_{n_k+1})+K_{\mathrm{rad}}. \quad (26)$$

For the second stage

$$(\theta^{k+1}_{n_k+1}-\theta^k_{n_{k+1}+1})Kl_{n_k}+(\theta^{k+1}_{n_{k+1}+2}-\theta^k_{n_{k+1}+1})\times Kr_{n_k}+\mathrm{Ko}K_{Vl}/\Delta\mathrm{Fo}-(\theta^{k+1}_{n_k}-\theta^k_{n_k+1})K_{Vh}/\Delta\mathrm{Fo}=0. \quad (27)$$

For the third stage when the layer is melting

$$(\theta^{k+1}_{n_k+1}-\theta^k_{n_{k+1}+1})Kl_{n_k}+\mathrm{Kix}^2_{n_k}+\mathrm{Ko}K_{Vl}/\Delta\mathrm{Fo}-(\theta^{k+1}_{n_k}-\theta^k_{n_k})K_{Vh}/\Delta\mathrm{Fo}=0. \quad (28)$$

For the third stage when the layer is solidifying

$$(\theta^{k+1}_{n_k+1}-\theta^k_{n_{k+1}+1})Kl_{n_k+2}+\mathrm{Kix}^2_{n_k+2}+\mathrm{Ko}K_{Vs}/\Delta\mathrm{Fo}=0. \quad (29)$$

Since the dependence of the current temperatures on their preceding values is determined implicitly by difference equations, calculation of the temperature field entails combined solution of these equations. The systems of linear algebraic equations obtained from the difference schemes are most effectively solved by fitting [7]. Specifically, the solution of Eqs. (19) and (24)–(29) is written in the form

$$\theta^{k+1}_i=\alpha_i\theta^{k+1}_{i+1}+\beta_i, \quad (30)$$

where α_i and β_i are auxiliary constants.

We find the fitting factors α_i and β_i corresponding to the left boundary point by solution of Eq. (25), written in the form in Eq. (30). Since $K_{\lambda,1}=K_{c\rho,1}=1$, we find that

$$\alpha_1=\frac{6\Delta\mathrm{Fo}/\Delta x^2}{1+6\Delta\mathrm{Fo}/\Delta x^2},\quad \beta_1=\frac{\theta^k_1}{1+6\Delta\mathrm{Fo}/\Delta x^2}. \quad (31)$$

To determine the other constants α_i and β_i, we convert Eq. (24) to the form in Eq. (30) and replace θ^{k+1}_{i-1} by $\alpha_{i-1}\theta^{k+1}_i+\beta_{i-1}$

$$\alpha_i=\frac{Kr_i\Delta\mathrm{Fo}/K_{V_i}}{1+[Kr_i+(1-\alpha_{i-1})Kl_i]\mathrm{Fo}/K_{V_i}},\quad \beta_i=\frac{\theta^k_i+\beta_{i-1}Kl_i\Delta\mathrm{Fo}/K_{V_i}}{1+[Kr_i+(1-\alpha_{i-1})Kl_i]\mathrm{Fo}/K_{V_i}}. \quad (32)$$

The dimensionless time step $\Delta\mathrm{Fo}$ is not known initially and must be determined from the boundary conditions in Eqs. (19) and (26) for the first stage; Eqs. (19), (26), and (27) for the second stage; and Eqs. (19), (28), and (29) for the third. If we replace $\theta^{k+1}_{n_{k+1}}$ by $\alpha_{n_{k+1}}\theta^{k+1}_{n_{k+1}+1}+\beta_{n_{k+1}}$ in Eqs. (26)–(29) and take account of Eq. (19), we obtain nonlinear equations, since $\Delta\mathrm{Fo}$ itself depends on $\alpha_{n_{k+1}}$ and $\beta_{n_{k+1}}$. These equations are solved by iteration, in the following form.

For the first stage

$$\Delta Fo' = [(\theta_{me} - \theta^k_{n_k+1})K_{V_{n_k+1}} - Kl_{n_k+1}(\alpha_{n_k}\theta_{me} + \beta_{n_k} - \theta_{me})\Delta Fo]/K_{rad}. \quad (33)$$

For the second stage

$$\Delta Fo' = -[(\alpha_{n_{k+1}}\theta_{me} + \beta_{n_{k+1}} - \theta_{me})Kl_{n_k}\Delta Fo + Ko K_{Vl} - (\theta_{me} - \theta^k_{n_k})K_{Vh}]/[(\theta^{k+1}_{n_{k+1}+2} - \theta_{me})Kr_{n_k}]. \quad (34)$$

For the third stage when the layer is melting

$$\Delta Fo' = -[(\alpha_{n_{k+1}}\theta_{me} + \beta_{n_{k+1}} - \theta_{me})Kl_{n_k}\Delta Fo + Ko K_{Vl} - (\theta_{me} - \theta^k_{n_k})K_{Vh}]/(Kix^2_{n_k}). \quad (35)$$

For the third stage when the layer is solidifying

$$\Delta Fo' = -\frac{Kix^2_{n_k+2}\Delta Fo + Ko K_{Vs}}{(\alpha_{n_{k+1}}\theta_{me} + \beta_{n_{k+1}} - \theta_{me})Kl_{n_k+2}} = 0. \quad (36)$$

When solidification of the next layer is impossible since the internal and external heat fluxes are equal, we obtain the following result from Eq. (29), taking into account that $\theta^k_{n_k+1} = \theta_{me}$

$$\Delta Fo' = -[Kl_{n_k+1}(\alpha_{n_k}\theta_{me} + \beta_{n_k} - \theta_{me})\Delta Fo]/(Kix^2_{n_k+1}). \quad (37)$$

Here ΔFo and $\Delta Fo'$ are the previous and subsequent approximations of the dimensionless time.

In each step of the iteration, by substituting the approximate value of ΔFo into Eqs. (33)–(37), we find $\alpha_{n_{k+1}}$ and $\beta_{n_{k+1}}$. The iteration ends when $|1 - \Delta Fo/\Delta Fo'| < \Delta$, where Δ is a specified value establishing the relative error of the time step.

To determine ΔFo from Eq. (34) in the second stage, we need to know $\theta^{k+1}_{n_{k+1}+2}$, which is the temperature of the right boundary. To that end, we use Eqs. (30) and (32) and the temperature at the surface of the pellet's molten component. This temperature may be obtained from Eq. (26) if we replace $\theta^{k+1}_{n_k}$ by $\alpha_{n_k}\theta^{k+1}_{n_k+1} + \beta_{n_k}$

$$\theta^{k+1}_{n_k+1} = \frac{\theta^k_{n_k+1} + (Kl_{n_k+1}\beta_{n_k} + K_{rad})\Delta Fo/K_{V_{n_k+1}}}{1 + Kl_{n_k+1}(1 - \alpha_{n_k})\Delta Fo/K_{V_{n_k+1}}}. \quad (38)$$

This mathematical model provides the basis for an algorithm and software that may be used in calculating the melting of a pellet close to the electrode, with allowance for heating by the arc.

When pellets are supplied to the furnace bath through a tubular electrode, they are first subjected to the thermal radiation from the arc and then melt in the metallic bath. Therefore, we use the following data in the calculation.

(1) For the pellets: radius $r_{pe} = 0.005$ m; thermal conductivity $\lambda_{pe} = 1.4$ W/m K; specific heat $c_{pe} = 878$ J/kg K; density $\rho_{pe} = 3000$ kg/m^3; initial temperature $t_{0pe} = 25$°C; melting point $t_{me.pe} = 1450$°C; latent heat of phase transformation (melting) $L_{pe} = 272200$ J/kg.

(2) For the molten pellet: thermal conductivity $\lambda_{m.pe} = 15$ W/m K; specific heat $c_{m.pe} = 878$ J/kg K; density $\rho_{m.pe} = 3000$ kg/m^3.

(3) For the metallic crust, thermal conductivity $\lambda_{cr} = 30$ W/m K; specific heat $c_{cr} = 687$ J/kg K; density $\rho_{cr} = 7250$ kg/m^3; melting point $t_{me.cr} = 1450$°C; latent heat of phase transformation (melting) $L_{cr} = 277000$ J/kg.

(4) For the metallic melt: temperature $t_{melt} = 2735$°C; convective heat-transfer coefficient $\alpha_{melt} = 1000$ W/m^2 K.

(5) For the arc: power 30 MW.

In calculating the dimensionless characteristics, the data for the pellet (c_{pe}, ρ_{pe}, λ_{pe}) are adopted as the initial thermophysical properties. The program for calculating the pellet melting close to the electrode is based on the proposed difference equations. From the system of implicit difference equations, the time step ΔFo and corresponding fitting factors α_i and β_i are first determined by iteration with direct fitting. Then, knowing the surface temperature on the basis of the boundary conditions, the required temperature distribution is determined by inverse fitting. Next, this calculation is repeated for the next time step, with a new number of coordinate increments. In the calculation of melting in the arc, determination of the time step is preceded by calculation of the temperature distribution in the melt that forms. The calculation ends when the number of coordinate steps reaches zero.

The algorithm employed in the program is shown in Fig. 2. The program consists of modules specifying the initial data from the preliminary calculations and three basic components corresponding to the number of periods of pellet melting.

(1) Surface heating of the pellet to the melting point as a result of the thermal radiation from the arc as it descends. The initial conditions employed here are the pellet radius, its initial temperature, and the condition of uniform heating.

(2) Pellet melting near the electrode as it descends in the arc. The initial dimensionless-temperature distribution over the pellet cross section $\theta(i, k)$ and the time step k are taken from the calculation for the preceding stage. The external heat flux from the arc is greater than the flux from the phase boundary. As a result, the pellet begins to melt, and a liquid layer forms at its surface. Thus, for the solid residue, the change in the number of coordinate increments is $\Delta n = -1$; the total number of increments for the pellet and melt remains unchanged. After the calculation for each time step, the condition for the end of melting in the arc is verified: $\tau > \tau_{de}$, where τ_{de} is the time for the pellet's descent in the arc. If this is not the case,

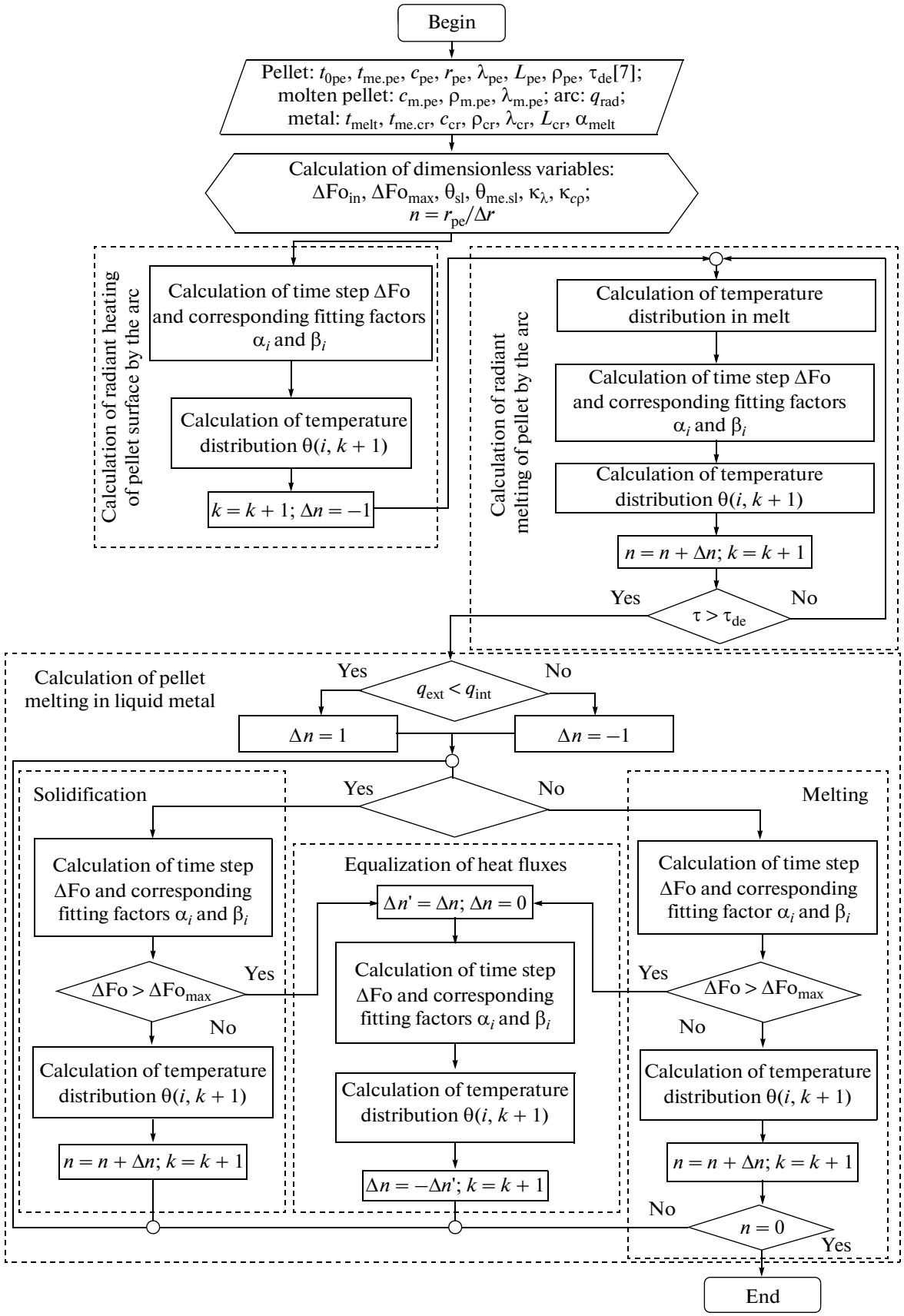

Fig. 2. Block diagram of the algorithm for calculating the melting of a pellet close to the electrode.

the program proceeds to the analogous calculation for the next time step.

(3) Melting of the pellet in the bath close to the electrode. (The formation of a metal crust is possible.) The initial dimensionless-temperature distribution over the pellet cross section $\theta(i, k)$, the time step k, and the number of coordinate steps for the pellet are taken from the calculation for the preceding stage. Since the initial heating of the pellet is not sufficient, the external heat flux q_{ext} may be less than the internal heat flux q_{int} from the phase boundary. As a result, solidification of a metal layer at its surface is possible. In that case, the calculation for this stage begins with the condition $\Delta n = 1$. Otherwise, melting occurs ($\Delta n = -1$).

If $\Delta n = 1$ initially, equations for calculating the solidification are selected (the left branch in Fig. 2). Since the pellet is gradually heated and the heat flux from the phase boundary declines, the time required for solidification of the last layer of melt is infinite. (Solidification of the last layer is impossible.) Thus, in calculating the next time step, when it exceeds the specified maximum time step ($\Delta Fo > \Delta Fo_{max}$), the program switches to calculation of the time step corresponding to equalization of the internal and external heat fluxes when $\Delta n = 0$ (the central branch in Fig. 2). Since the flux from the phase boundary is less than the external heat flux, melting begins, and the change in the number of coordinate steps changes sign: $\Delta n = -\Delta n' = -1$. (Here $\Delta n'$ is the change in the time step for calculation of the equalization of the heat flux.) Given that $\Delta n = -1$, the equation for the calculation of melting may be selected (the right branch in Fig. 2). After calculating each time step, the condition corresponding to the end of melting is verified: $n = 0$. If it is not satisfied, the program switches to the calculation for the next time step.

This algorithm is incorporated in Matlab software. The model is tested by comparing the calculation results for the crust thickness on tin samples immersed in hot melt [8, 9] with experimental data from [6]. For pellets supplied through a tubular electrode to the melt close to the arc, the melting time is a quarter of that for pellets melting in the slag (that is, with no influence of the arc), according to the data in [8, 9]. When the pellet is supplied to the slag, the crust formed extends over 25% of its radius, while the period in which the crust exists is 35% of the melting time. For pellets supplied through a tubular electrode, the crust is less than a third as much, and the period in which the crust exists is no more than 20% of the melting time; with a large heat-transfer coefficient, no crust is formed at all.

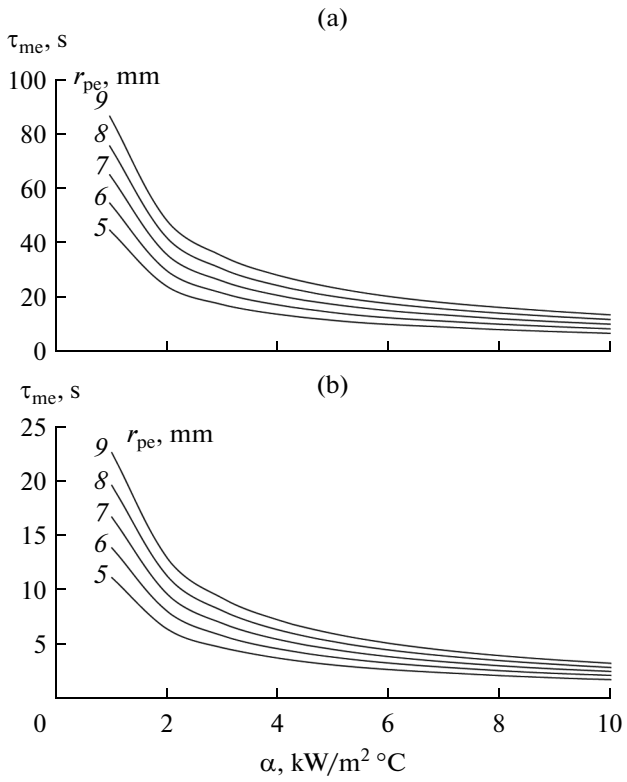

Fig. 3. Dependence of the melting time on the pellet size and the heat-transfer coefficient when the pellet is supplied to the slag (a) and in the vicinity of the electrode (b).

The pellet temperature was studied dynamically in the course of heating and melting in [8]. It was found that, when the pellet melts within the slag, it is uniformly heated at the end of crust formation. By contrast, for pellets supplied through a tubular electrode, there is a temperature gradient over its cross section. In Fig. 3, we show the melting time of the pellet in these two cases, as a function of its size and the heat-transfer

Constants in the dependence of the pellet's melting time on the heat-transfer coefficient, with pellet supply to the slag (A) and to the metal in the vicinity of the electrode (B)

r_{pe}	A		B	
	a	b	a	b
9	85.176	−0.8	23.097	−0.861
8	74.118	−0.801	19.999	−0.854
7	63.379	−0.801	16.977	−0.846
6	53.03	−0.804	14.047	−0.838
5	43.073	−0.809	11.174	−0.827
	$a = 10.53r_{pe} - 9.951$; $b = 0.0021r_{pe} - 0.8177$		$a = 2.98r_{pe} - 3.8$; $b = -0.0084r_{pe} - 0.7864$	

coefficient, with the corresponding melt temperatures. Each curve in Fig. 3 may be described by a power law

$$\tau_{me} = a\alpha^{b}, \quad (39)$$

where a and b are constants, whose values are presented in the table. These constants depend linearly on the pellet radius. Substituting the values of a and b into Eq. (39), we obtain equations for the melting time of a pellet in slag and in the vicinity of the electrode.

CONCLUSIONS

Our results provide a better understanding of the heating and melting of the pellets, with allowance for the radiant action of the electrical arc, the formation of a solid crust, and the conditions of pellet delivery. A mathematical model of melting when the pellet is supplied in the vicinity of the electrode permits prediction of the melting time.

Simulation indicates that the melting of pellets close to the electrodes offers certain benefits. Thus, the melting time is about a quarter of that for melting within the slag; the crust thickness is less than a third as much; and the period in which the crust exists is no more than 20% of the melting time. With a large heat-transfer coefficient, no crust is formed at all. When the pellet is supplied to the slag, the crust formed extends over 25% of its radius, while the period in which the crust exists is 35% of the melting time.

If the pellet temperature is studied dynamically in the course of heating and melting, we find that, when the pellet melts within the slag, it is uniformly heated at the end of crust formation. By contrast, for pellets supplied through a tubular electrode, there is a temperature gradient over its cross section.

We have obtained equations for the melting time of a pellet in slag and in the vicinity of the electrode, with the corresponding melt temperatures.

REFERENCES

1. Sazonov, A.V., Merker, E.E., and Chermenev, E.A., Melting of pellets in the area where an electric arc acts on slag–metal melt, *Byull. Chern. Metall.*, 2011, no. 8, pp. 62–64.
2. Chermenev, E.A., Merker, E.E., and Kharlamov, D.A., Simulation of heat transfer, heating, and melting of pellets in the bath of an arc furnace, *Izv. Vyssh. Uchebn. Zaved., Chern. Metall.*, 2013, no. 5, pp. 67–68.
3. Merker, E.E., Karpenko, G.A., and Chermenev, E.A., Russian patents 2 487 306 and 2 487 172, *Byull. Izobret.*, 2013, no. 19.
4. Nugumanov, R.V., Prototopov, E.V., Kharlashin, P.S., and Bakst, V.Ya., Interaction of steel scrap with ferrocarbon melt in diffusional and heating conditions, *Steel Transl.*, 2009, vol. 39, no. 8, pp. 624–628.
5. Merker, E.E., Sazonov, A.V., and Grishin, A.A., Electrosmelting of reduced pellets in the bath of an arc furnace, *Izv. Vyssh. Uchebn. Zaved., Chern. Metall.*, 2008, no. 2, pp. 31–33.
6. Grishin, A.A., Merker, E.E., and Kochetov, A.I., Formation of a coating on the pellet surface at immersion in melt, *Izv. Vyssh. Uchebn. Zaved., Chern. Metall.*, 2006, no. 1, pp. 69–70.
7. Artyunov, V.A., Bukhmirov, V.V., and Krupennikov, S.A., *Matematicheskoe modelirovanie teplovoi raboty promyshlennykh pechei: uchebnik dlya vuzov* (Thermal Simulation of Industrial Furnaces: A University Textbook), Moscow: Metallurgiya, 1990.
8. Chermenev, E.A., Merker, E.E., and Stepanov, V.A., Model of the heating and melting of iron-ore pellets in an arc furnace, *Izv. Vyssh. Uchebn. Zaved., Chern. Metall.,* 2014, no. 1, pp. 65–69.
9. Merker, E.E., Chermenev, E.A., and Sazonov, A.V., Effectiveness of smelting of reduced pellets continuously supplied to an arc furnace, *Izv. Vyssh. Uchebn. Zaved., Chern. Metall.*, 2012, no. 5, pp. 14–17.

Translated by Bernard Gilbert